Digest Journal of Nanomaterials and Biostructures Vol. 12, No. 3, July - September 2017, p. 829 - 839

NICKEL DOPED NANOROD TITANIUM DIOXIDE PHOTOCATALYST WITH ENHANCED VISIBLE LIGHT PHOTOCATALYTIC PERFORMANCE

S. BUDDEE[a], C. SUWANCHAWALIT[b*], S. WONGNAWA[c]
[a]*Department of General Science, Faculty of Education, Nakhon Si Thammarat Rajabhat University, Nakhon Si Thammarat, Thailand 80280*
[b]*Department of Chemistry, Faculty of Science, Silpakorn University, Sanam Chandra Palace Campus, Nakornpathom, Thailand 73000*
[c]*Department of Chemistry, Faculty of Science, Prince of Songkla University, Hat Yai, Songkhla, Thailand 90112*

Ni-doped nanorod TiO_2 photocatalysts were prepared by mixing a nickel solution with TiO_2 powders via a modified impregnation method. In this study 5, 10, 25 mol% of Ni doping were studied. The physical properties of the Ni-doped TiO_2 photocatalysts were studied by several techniques such as X-ray powder diffraction (XRD), scanning electron microscopy (SEM), Fourier-transformed infrared spectroscopy (FT-IR), X-ray photoelectron spectroscopy (XPS), and UV-Vis diffused reflectance spectroscopy (DRS). XRD patterns showed that pure TiO_2 sample and Ni-doped TiO_2 samples were anatase phase. No diffraction patterns of Ni peaks were observed. The crystallite size of Ni-doped TiO_2 samples were examined using the Scherrer equation. SEM results revealed that the pure TiO_2 and Ni-doped TiO_2 nanoparticles had rod-like structures. The FT-IR spectra showed the characteristic bands of the titania and hydroxyl groups on the surface of the titania. The XPS results confirmed the existence of Ni, Ti, O, C elements. Nickel dopants existed in the form of nickel oxide on the surface of TiO_2 sample. The DRS spectra revealed that the absorbance of Ni-doped TiO_2 samples extended into the visible region. The photocatalytic properties of Ni-doped TiO_2 photocatalysts were evaluated from the degradation of methylene blue under visible light irradiation. The Ni-doped TiO_2 samples exhibited higher photocatalytic performance than the pure TiO_2 sample under visible light irradiation. This could be due to the electron trap level promoting the separation of charge carriers and the oxygen vacancies inducing the visible light absorption. A possible photocatalytic mechanism has also been proposed.

(Received May 3, 2017; Accepted August 18, 2017)

Keywords: Ni-doped TiO_2, Visible photocatalyst, Degradation of methylene blue

1. Introduction

Titanium dioxide (TiO_2) is an effective n-type semiconducting materials generally used for decomposing organic pollutants, photogeneration of hydrogen from water, and solar energy utillization [1-4]. However, there are some drawbacks such as high recombination rate of photogenerated electron-hole pairs and low absorption ability for solar energy. To improve the photocatalytic efficiency, the main route has been made to shift the light absorption toward visible light and extend the lifetime of the photogenerated electron-hole pairs [5-6]. Various strategies have been used to enhance the photocatalytic activity like doping with transition metals (Fe [7], Cu [8], Ni [9], Cr [10])/main group elements (C [11], N [12], S [13], F [14]), coupling TiO_2 with other narrow bandgap semiconductors ($BiVO_4$ [15], Cu_2O [16], Fe_3O_4 [17], $CoFe_2O_4$ [8]), and dye sensitized TiO_2 [19-22]. Many researches have confirmed that transition metal doping could

---

[*] Corresponding author: suwanchawalit_c@su.ac.th

extend the light absorption of TiO_2 into visible region. Dopant ion could act as donor or acceptor states, promotes the transfer and separation of electrons and holes and thereby enhance the visible photocatalytic performance [5, 7, 10, 16, 19]. Among the various dopants, nickel has been known to be an effective dopant for improving photocatalytic activity of TiO_2 photocatalyst.

In the present work, we investigate the effect of doping nickel into TiO_2 photocatalyst with respect to the crystalline phase, optical properties, and photocatalytic activity. The synthesized Ni-doped TiO_2 photocatalysts were characterized by various physical techniques such as X-ray diffraction spectrometry (XRD), scanning electron microscopy (SEM), Fourier-transformed infrared spectroscopy (FT-IR), X-ray photoelectron spectroscopy (XPS), and UV-Vis diffused reflectance spectroscopy (DRS). The nickel dopant plays an important role in extending the absorbance into the visible region. The photocatalytic activity of the as-prepared Ni-doped TiO_2 photocatalyst was tested using methylene blue (MB) as a model pollutant and compared with pure TiO_2. The generated hydroxyl radical ($^{\bullet}OH$) during the photocatalytic experiment was investigated.

2. Experimental procedure

2.1 Preparation of nanorod TiO_2 photocatalyst

The nanorod TiO_2 nanoparticles were prepared via a one-pot hydrothermal method. Briefly, 10.00 g of anatase TiO_2 powder was mixed with 50 mL of 10 M NaOH aqueous solution and stirred for 10 minutes. Then the mixture was transferred to a Teflon-lined autoclave and kept at 120 ^{o}C in a furnace for 15 h. Finally, the precipitate was collected, centrifuged, and washed several times with distilled water and ethanol, then dried at 80 ^{o}C for 24 h.

2.2 Preparation of Ni-doped nanorod TiO_2 photocatalyst

Briefly synthesis of Ni doped TiO_2 via impregneation process, 1.00 g of pure TiO_2 was dispersed into 50 mL of $Ni(NO_3)_2.6H_2O$ solution with different concentrations of 5, 10, and 25mol% for 3 h. After 3 h, the precipitate was filtered and washed with distilled water and ethanol and dried at 80 ^{o}C for 24 h.

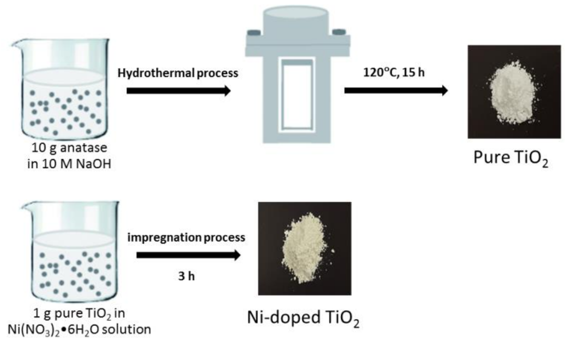

Fig. 1 Synthetic route of pure TiO_2 and Ni-doped TiO_2 samples

2.3. Characterizations

The crystal structure and crystallite size were identified by X-ray diffraction (XRD) patterns recorded on a Rigaku MiniFlex II X-Ray diffractometer with Cu Kα radiation (1.5406 Å) from 20° to 80° (2θ). The chemical composition and valence states of Ni-doped TiO_2 samples were determined by X-ray photoelectron spectroscopy (XPS: AXIS Ultra DLD, Kratos Analytical Ltd.). Fourier-transformed infrared (FT-IR) spectra were recorded on a Perkin Elmer Spectrum Bx spectrophotometer in the range 400-4000 cm^{-1} using the KBr pellet technique. The morphologies and microstructure were investigated using a scanning electron microscopy (SEM, JEOL model

JSM-7800F). Optical absorption property and band gap energy were determined using a Shimadzu UV-2401 spectrophotometer. The hydroxyl radical ($^{\bullet}$OH) measurement was investigated using fluorescence spectrometer (Perkin Elmer LS-50B Luminescence Spectrometer).

2.4. Photocatalytic experiment

The photocatalytic performances of the prepared pure TiO_2 and Ni-doped TiO_2 samples were evaluated by the photocatalytic degradation of methylene blue under visible light using 18W fluorescence lamp as a visible light source [6, 23-24]. Briefly, a 0.05 g of sample was added to 50 mL methylene blue solution (MB, $1.0x10^{-5}$M). The suspension was stirred in the dark for 1 h to allow it to reach adsorption equilibrium then was irradiated under fluorescence lamp for the pre-determined time. At the time interval, the sample was collected (2 mL) and centrifuged to separate the photocatalysts. The residual concentration of methylene blue solution was monitored by the change in absorbance of the dye at 664 nm using a UV-Vis spectrophotometer (Analytik Jena GmbH).

The photocatalytic activity of the catalysts was measured in terms of the degradation efficiency (%) by the following equation:

$$The\ degradation\ efficiency\ (\%) = \frac{A_0 - A_i}{A_0} \times 100 \tag{1}$$

where A_0 is the initial concentration of MB and A_i is the concentration of MB at any time interval.

2.5. Hydroxyl radical measurement

The amount of hydroxyl radical of the prepared pure TiO_2 and Ni-doped TiO_2 samples were evaluated by using terepthalic acid as $^{\bullet}$OH scavenger [25]. The experimental procedures were similar to the measurement of photocatalytic activity except that the methylene blue solution was replaced by an aqueous solution of $5.0x10^{-4}$M terepthalic acid and $2.0x10^{-3}$ M sodium hydroxide solution. The visible light irradiation was continuous and sampling was performed at given time intervals for fluorescence analysis (Perkin Elmer LS-50B Luminescence Spectrometer). The fluorescence product gave a peak at 425 nm by using excitation wavelength 315 nm.

3. Results and discussion

3.1. Microstructure and composition

The XRD diffraction patterns of the prepared pure TiO_2 and Ni-doped TiO_2 samples are shown in Fig. 2. It can be seen that all diffraction peaks of pure TiO_2 and Ni-doped TiO_2 samples correspond to the anatase phase (JCPDS 21-1271) [6]. No diffraction peaks corresponding to nickel species such as metallic Ni, nickel oxides (NiO, NiO_2 and Ni_2O_3), or nickel titanate ($NiTiO_3$) were observed due to the amount of nickel content on the surface of TiO_2 was too low to be detected. From the obtained peaks at $2\theta = 25.5°$, the crystallite sizes were calculated using the Scherrer formula (Equation 2) and are given in Table 1.

$$D = \frac{K\lambda}{\beta cos\theta} \tag{2}$$

where D is the crystallite size; K is the shape factor (0.9); λ is the 0.154 nm (Cu Kα radiation); β is the full width at half maximum and θ is reflection angle.

The crystallite size of Ni-doped TiO_2 samples are smaller size than that of pure TiO_2 sample, since Ni doping can suppress its crystal growth. It has been reported that TiO_2 doped with transition metals such as Ni and Fe possesses smaller particle sizes [26-27]. The decrease in grain growth could be attributed to the formation of Ni-O-Ti bond in the Ni-doped TiO_2 samples, which inhibits the growth of the crystal grains. The substitution of Ni^{2+} for Ti^{4+}should result in peak shift in the XRD, however, there is no obvious shift for the diffraction peaks of the TiO_2, indicating that no solid solution between dopant and host matrix is formed. With regards to the absence of such shifts in the recorded XRD, one can expect that the segregation of dopants in the grain boundaries of TiO_2 or incorporation of only an insignificant quantity in the substitutional Ti sites was happened [28]. Therefore, Ni dopants likely did not substitute into the crystal structure of titania to form a solid solution, this fact is also confirmed by XPS analysis.

Table 1 Calculated crystallite size and band gap energy of the prepared pure TiO_2 and Ni-doped TiO_2 samples

TiO_2 photocatalysts	Crystallite size (nm)	Band gap energy (eV)
Pure TiO_2	4.62	3.19
5%Ni-TiO_2	2.87	3.12
10%Ni-TiO_2	1.97	3.10
25%Ni-TiO_2	4.14	3.01

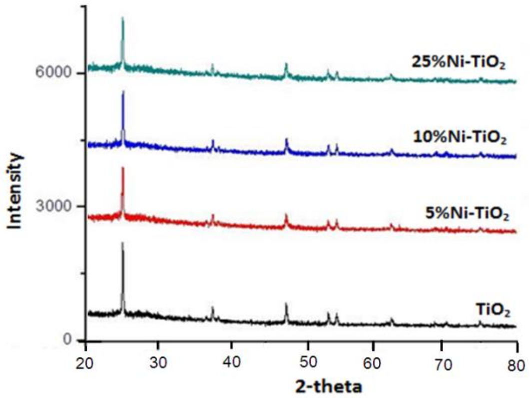

Fig. 2. XRD patterns of pure TiO_2 and Ni-doped TiO_2 samples

XPS was used to study the composition and oxidation state in the products (Fig. 3) which showed the full survey and high resolution XPS data for the Ni-doped TiO_2 sample. In the XPS survey spectrum, Ti, O, Ni, C were detected in the product. The high resolution XPS spectra products (Fig. 3b) showed the Ti $2p_{3/2}$ and Ti $2p_{1/2}$ peaks at 459 and 464 eV, respectively, corresponding to the Ti^{4+} ion in the sample [9, 29]. The Ni 2p spectra were detected in two groups: the first group Ni $2p_{3/2}$ and Ni $2p_{1/2}$ appeared at 856 and 873.8 eV, respectively, indicating the presense of NiO [29-30]; the second group appeared at 862 and 880 eV indicating the presense of Ni_2O_3 [29-30]. Therefore, nickel atoms are existed in the form of nickel oxide on the surface of TiO_2 sample. The existence of Ni^{2+} and Ni^{3+} gave the advancetage of enhanced separation of electron-hole pairs [29, 31]. The O 1s spectra were deconvoluted into two components: oxygen in titanium lattice and surface hydroxyl group appeared at 531 and 533 eV, respectively [29-30]. The C 1s spectra composed of two components which were assigned to CH_x and C-OH as hydrocarbon impurities during preparation [32-33].

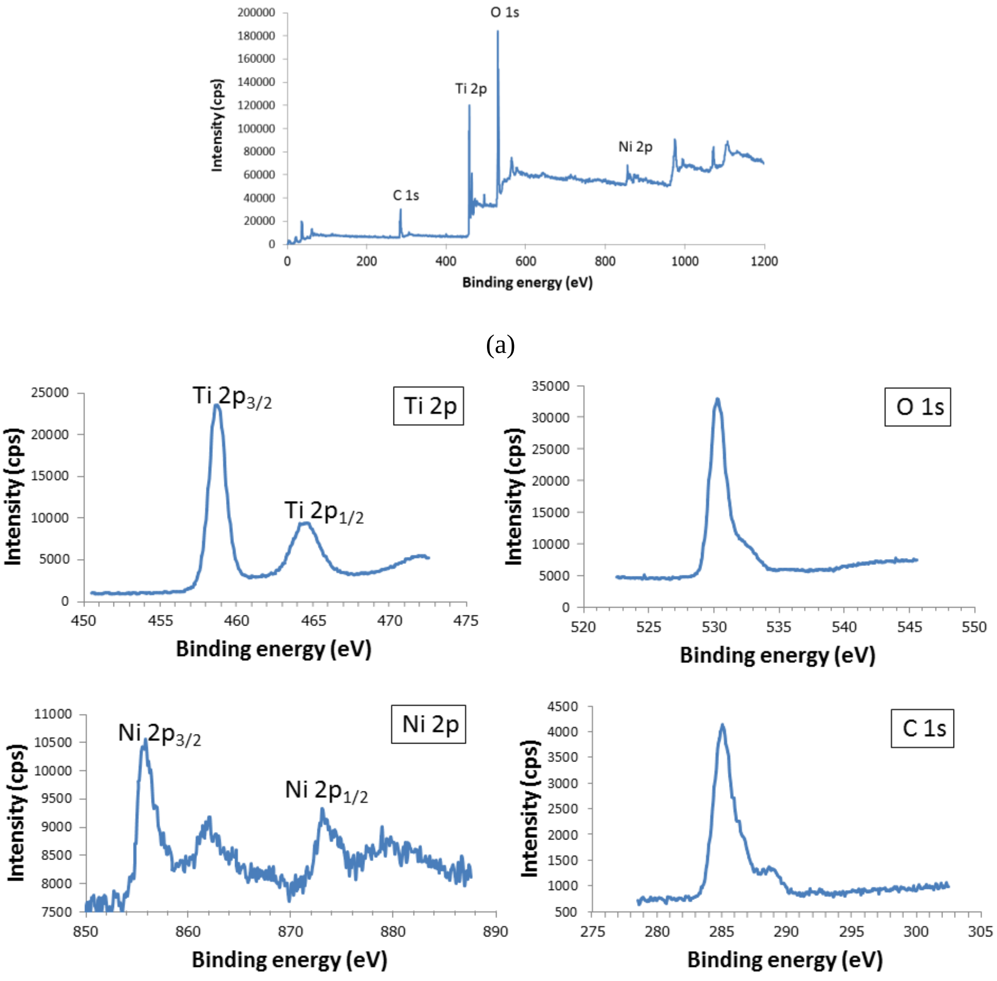

(a)

(b)

Fig. 3 XPS spectra of Ni-doped TiO_2 (a) survey spectrum
(b) high-resolution of Ti 2p, O 1s, C 1s and Ni 2p spectra

The surface chemical compositions was investigated with Fourier-transformed infrared spectroscopy (FT-IR) and the results are shown in Fig. 4. Both pure TiO_2 and Ni-doped TiO_2 samples revealed vibration bands of Ti-O bond (in the range of 400-800 cm^{-1}) [6] and the surface adsorbed H_2O (in the range of 3000-3600 cm^{-1} [6] and at 1640 cm^{-1} [6]). Most samples were exhibited characteristic band of alkyl group $[-(CH_2)_n-]$ (weak bands at 2923 cm^{-1} [11]) indicating its presence on the surface of these synthesized samples.

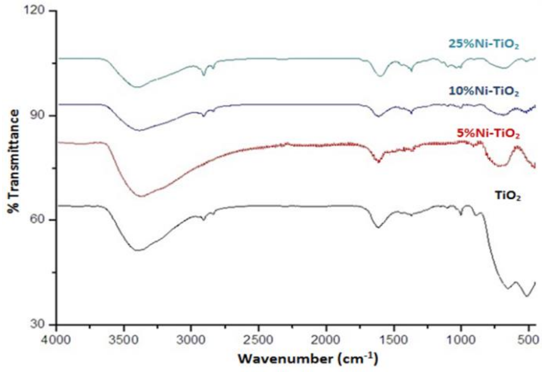

Fig. 4 FT-IR spectra of pure TiO_2 and Ni-doped TiO_2 samples.

The morphologies of pure TiO_2 and Ni-doped TiO_2 samples were evaluated by SEM technique illustrated in Fig. 5. As shown in the figure, most of the particles have rod shape with uniform diameter and highly agglomerated on higher Ni doping content. The diameter of pure TiO_2 and Ni-doped TiO_2 samples are approximately 50-60 nm. Comparing these Ni-doped TiO_2 shapes with pure TiO_2 sample revealed the same morphologies that could be due to the impregnation method used in this experiment. This result is in accordance with the fact that Ni doping could grow on the titania surface.

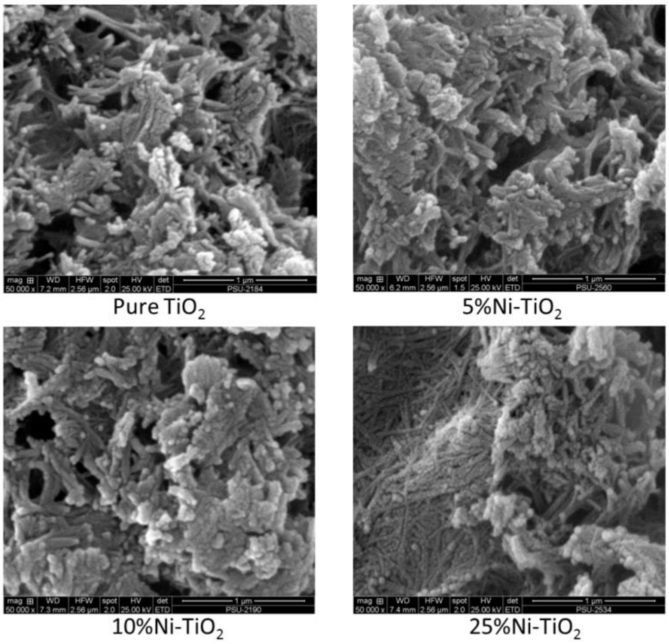

(a)

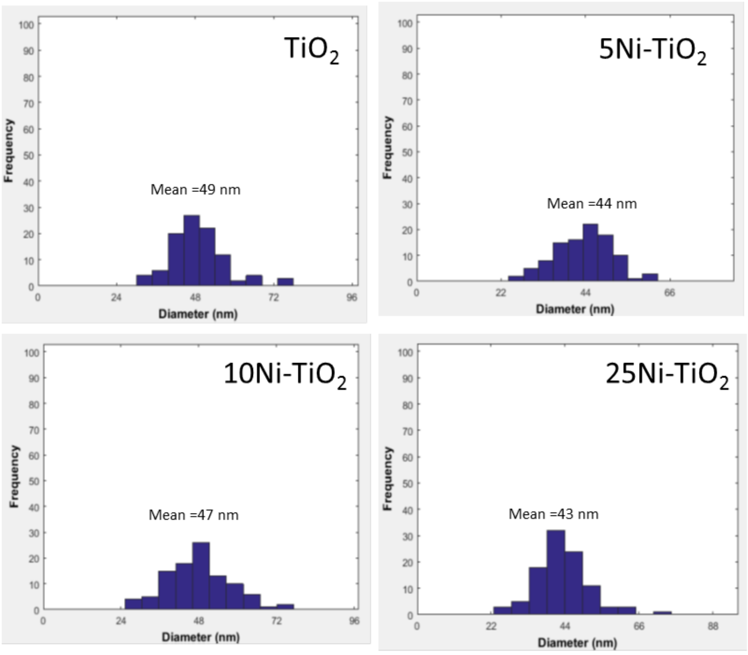

(b)

Fig. 5 SEM images (a) and diameter size distributions of pure TiO_2 and Ni-doped TiO_2 samples (b).

3.2. Optical property and photocatalytic activity

The optical properties and band gap energy of the prepared pure TiO_2 and Ni-doped TiO_2 samples were investigated with the diffused reflectance UV-vis spectra (DRS), as shown in Fig. 6. According to the spectra, all Ni-doped TiO_2 samples exhibited more extended photoabsorption into visible light region than the pure TiO_2 sample, which should favor the possibility of high photocatalytic efficiency of these photocatalysts under visible light**.**

The band gap energies of the prepared pure TiO_2 and Ni-doped TiO_2 samples were obtained from the wavelength at the intersection point of the vertical and horizontal part of the spectrum, using equation (3):

$$E_g = \frac{hc}{\lambda} = \frac{1240}{\lambda} \tag{3}$$

where Eg is the band gap energy (eV); h is the Plank's constant (6.626×10^{34} Js); c is the light velocity (3×10^8 m/s) and λ is the wavelength (nm). The calculated band gap energy of the prepared Ni-doped TiO_2 samples decreased when compared with pure TiO_2 as shown in Table 1.

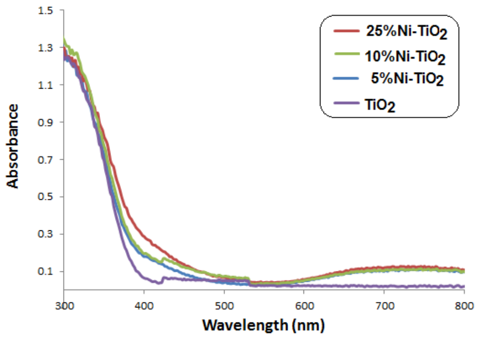

Fig. 6. The absorption spectra of pure TiO_2 and Ni-doped TiO_2 samples

The photocatalytic degradation of methylene blue using the prepared pure TiO_2 and Ni-doped TiO_2 samples was examined under visible light irradiation. The results are shown in Fig. 7 where one can see that the visible light photocatalytic activities of all Ni-doped TiO_2 are higher than pure TiO_2 in 5 h of irradiation. The Ni-doped TiO_2 can generate more hydroxyl radicals than pure TiO_2 due to the good optical absorption in the visible region with more hydroxyl group adsorbed on the catalyst surface giving rise to a higher photocatalytic performance. In addition, the nickel species can reduce the recombination of the photo-generated electron-holes, leading to improved photo-conversion efficiency [34]. The doping concentration of 5mol% showed the best performance among all samples. At higher Ni dopant concentrations, the Ni^{2+} dopant could become recombination centers of electron-holes resulting in high recombination rate, hence, the lower degradation efficiency [34].

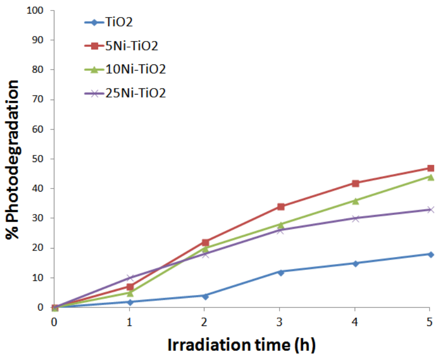

Fig. 7. Comparison of the photodegradation efficiencies of methylene blue using the prepared pure TiO_2 and Ni-doped TiO_2 samples under visible light irradiation

The fluorescence probing method was adopted to detect the hydroxyl radical (${}^\bullet$OH) with terepthalic acid in photocatalytic reactions in aqueous suspension system [25, 35]. This method relies on the PL signal arising from the hydroxylation of terepthalic acid with ${}^\bullet$OH to produce a highly fluorescent product, 2-hydroxyterepthalic acid through the reaction (4). The PL intensity of 2-hydroxyterepthalic acid is proposional to the amount of ${}^\bullet$OH produced in water.

$$C_6H_4(COOH)_2 + {}^\bullet OH \rightarrow C_6H_4(COOH)_2OH^\bullet \qquad (4)$$

As shown in Fig.8, significant fluorescent intensity from 2-hydroxyterepthalic acid was detected at 425 nm. The capability of forming OH radicals per unit mass of prepared TiO_2 powder was evaluated. All Ni%-doped TiO_2 generated higher concentration of hydroxyl radical than the pure TiO_2 under visible light irradiation.

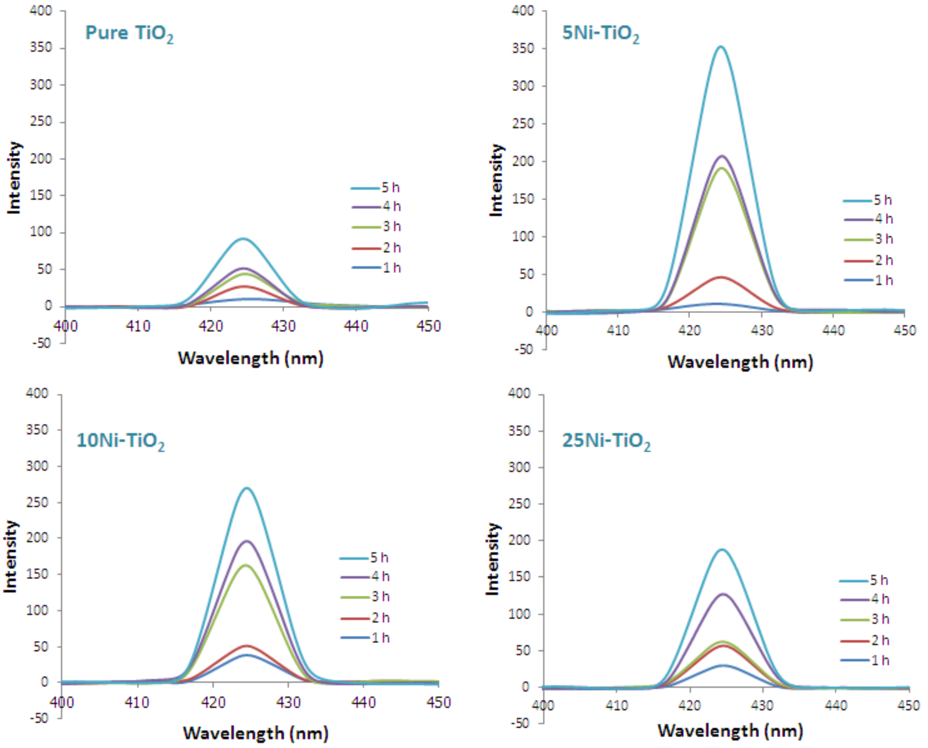

Fig. 8 Comparison of the photodegradation efficiencies of methylene blue using the prepared pure TiO_2 and Ni-doped TiO_2 samples under visible light irradiation.

3.3. Possible mechanism pathway

The photocatalytic degradation of dye exhibited by Ni doped nanorod TiO_2 under visible light irradiation may be explained as shown in Scheme 1.

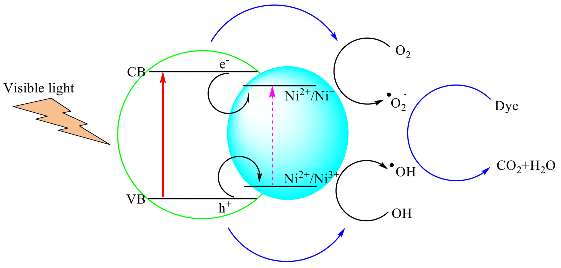

Scheme 1. Possible mechanism for photocatalytic activity of Ni-TiO_2 under visible light irradiation.

From DRS results, the absorption band ~389 nm can be attributed to the band gap excitation of nanorod TiO_2 which corresponds to band to band transition from Ti 3d to O 2p levels [36]. The doped samples showed a significant shift in the band gap absorption to the longer wavelength, due to the introduction of electronic level which forms lowest unoccupied molecular orbital within the band gap states of TiO_2. In the case of Ni-TiO_2, interband transition arises from the valence band to t_{2g} level of Ni (3d), since 3d level of Ni is located at the bottom of conduction band [37-38] (Scheme 1). The shift in the band gap absorption increased with increase in Ni concentration (379 to 412 nm). It has been proved that transition metal ions present in a suitable oxidation state can additionally introduce d-d transitions in the UV-vis spectra [39]. Hence, the absorption of Ni-TiO_2 catalysts in the visible region is partially attributed to the d-d transition of Ni. As mentioned in the XPS result which revealed the existence of Ni^{2+} and Ni^{3+} species in the doped-TiO_2 samples. The Ni^{3+} that present will trap the photogenerated electron to form Ni^{2+} during the irradiation process, thus decrease the recombination rate. Then, the formed Ni^{2+} will eventually react with photogenerated h^+ and turns back to Ni^{3+}. Therefore, it is deduced that Ni dopant not only facilitate the excited electron transfer and increase the photo quantum efficiency, but also played the role of stabilizer by trapping the photogenerated h^+, thus improve the photocatalytic activity and stability [31, 37].

When illuminated with visible light, TiO_2 photocatalyst generates $e^- + h^+$ pair (Eq (5)). In Eq. (6), trace of O_2 in the system has been adsorbed onto the surface of the catalyst and reacts with e^- to become the superoxide anion – a precursor to Eqs. (7)–(9). The pollutant molecules are attacked by the very reactive $^{\bullet}OH$ and destroyed, Eq (10)

$$TiO_2 + h\nu \rightarrow e^- + h^+ \tag{5}$$

$$O_{2(ads)} + e^- \rightarrow O_2^{\bullet-} \tag{6}$$

$$O_2^{\bullet-} + H^+ \rightarrow HO_2^{\bullet} \tag{7}$$

$$2HO_2^{\bullet-} \rightarrow H_2O_2 + O_2 \tag{8}$$

$$H_2O_2 + e^- \rightarrow {}^{\bullet}OH + OH^- \tag{9}$$

$$\text{Dye} + {}^{\bullet}OH \rightarrow \text{degradation products} \tag{10}$$

Moreover, Ni dopant also exhibits trapping and detrapping mechanism leading to enhancement of photoreactivity as shown in Eqs (11)–(16) [36].

$$Ni^{2+} + e^- \rightarrow Ni^+ \tag{11}$$

$$Ni^+ + O_{2(ads)} \rightarrow Ni^{2+} + O_2^{\bullet-} \tag{12}$$

$$Ni^+ + h^+ \rightarrow Ni^{2+} \tag{13}$$

$$Ni^{2+} + h^+ \rightarrow Ni^{3+} \tag{14}$$

$$Ni^{3+} + e^- \rightarrow Ni^{2+} \tag{15}$$

$$Ni^{3+} + OH^- \rightarrow Ni^{2+} + {}^{\bullet}OH \tag{16}$$

4. Conclusions

Ni-doped nanorod TiO_2 photocatalyst was successfully prepared by modified impregnation method. Different concentrations of Ni doping were attempted. The physical properties of the Ni-doped TiO_2 photocatalyst were studied by several techniques such as XRD, XPS, SEM, FT-IR, and DRS. The TiO_2 phase in both pure TiO_2 and Ni-doped TiO_2 samples were anatase. SEM images revealed that the rod-like structures of pure TiO_2 have larger size than rod-like Ni-doped TiO_2 samples, which are in good agreement with the crystallite size obtained from XRD results. The DRS results revealed that the Ni-doped TiO_2 samples showed extended absorbance into the visible region.

The photocatalytic performances of the pure TiO_2 sample and Ni-doped TiO_2 photocatalysts were evaluated by the degradation of methylene blue under visible light irradiation. The Ni-doped TiO_2 samples exhibited higher photocatalytic performance than the pure TiO_2 sample under visible light irradiation. The formation of hydroxyl radical was evaluated by PL technique. All Ni-doped TiO_2 samples produced higher concentration of hydroxyl radical than the pure TiO_2 under visible light irradiation. Moreover, Ni dopant also played the role of stabilizer by trapping the photogenerated h^+, thus improved the photocatalytic activity and stability.

Acknowledgments

The author would like to thank the Faculty of Science, Silpakorn University, Nakornpathom, Thailand for financial support (Grant No. SRF-JRG-2559-02).

References

[1] A. Fujishima, K. Honda, Nature. **238**, 37 (1972).
[2] M.R. Hoffmann, S.T. Martin, W. Choi, D.W. Bahnemann., Chem.Rev. **95**, 69 (1995).
[3] P.V. Kamat, Chem. Rev. **93**, 267 (1993).
[4] Y.H. Zheng, C.Q. Chen, Y.Y. Zhan, X.Y. Lin, Q. Zheng, K.M. Wei, J.F. Zhu, J. Phys. Chem. C. **112**, 10773 (2008).
[5] D. Chen, Y. Li, J. Zhang, J.Z. Zhou, Y. Guo, H. Liu, Chem. Eng. J. **185– 186**, 120 (2012).
[6] C. Suwanchawalit, S.Wongnawa, P. Sriprang, P. Meanha, Ceram. Int. **38**, 5201 (2012).
[7] H. Moradi, A. Eshaghi, S. R. Hosseini, K. Ghani, Ultrasonics Sonochemistry **32**, 314 (2016).
[8] C. Liu, J. Wang, W. Chen, C. Dong, C. Li, Chem. Eng. J. **280**, 588 (2015).
[9] Q. Wang, Z. Qin, J. Chen, B. Ren, Q. Chen, Y. Guo, X. Cao, Appl. Surf. Sci. **364**, 1 (2016).
[10] S. Buddee, S. Wongnawa, U. Sirimahachai, W. Puetpaibool, Materials Chemistry and Physics, **126**, 167 (2011).
[11] J. Liu, L. Han, N. An, L. Xing, H.Ma, L. Cheng , J.Yang ,Q. Zhang, Applied Catalysis B: Environ. **202**, 642 (2017).
[12] Y. Cong, J. Zhang, F. Chen, M. Anpo, J. Phys. Chem. C. **111**, 6976 (2007)
[13] X. Chen, D.H. Kuo, D.Lu, Advanced Powder Technology. **28**, 1213 (2017).
[14] W. Yu, X. Liu, L. Pan, J. Li , J. Liu, J. Zhang , P. Li, C. Chen, Z. Sun, Appl. Surf. Sci. **319**, 107 (2014).
[15] A.M. Cruz, U.M.C. Perez, Mater. Res. Bull. **45**, 135 (2010).
[16] L. Huang, F. Peng, H. Wang, H. Yu, Z. Li. Cat. Commun. **10**, 1839 (2009).
[17] L. Tan, X. Zhang, Q. Liu , X. Jing, J. Liu, D. Song, S. Hu, L. Liu, J. Wang, Colloids Surf. A: Physicochem. Eng. Aspects. **469**, 279 (2015)
[18] P. Sathishkumar, R. V. Mangalaraja, S. Anandan , M. Ashokkumar, Chem.Eng. J. **220**, 302 (2013).
[19] A. Zyoud, N. Zaatar, I, Saadeddin, M.H. Helal, G. Campet, M. Hakim, D. Park, H.S. Hilal, Solid State Sci. **13**, 1268 (2011).
[20] K. Hara, H. Sugihara, Y. Tachibana, A. Islam, M. Yanagida, K. Sayama, H. Arakawa, Langmuir. **17**, 5992 (2001).
[21] S. Hao, J.H. Wu, Y. Huang, J. Lin, Sol. Energy. **80**, 209 (2006).
[22] E. Yamazaki, M. Murayama, N. Nishikawa, N. Hashimoto, M. Shoyama, O. Kurita, Sol. Energy. **81**, 512 (2007).
[23] C. Suwanchawalit, V. Somjit, Digest Journal of Nanomaterials and Biostructures. **10(2)**, 705 (2015).
[24] C. Suwanchawalit, V. Somjit, Digest Journal of Nanomaterials and Biostructures. **10(3)**, 769 (2015).
[25] O. Mehraj, N. A. Mir, B. M. Pirzada, S.Sabir , M. Muneer, J. Molecular Catal. A:

Chem. **395**, 16 (2014).
[26] M. Kang, J. Molecular Catal.A: Chem. **197**, 173 (2003).
[27] L. Pan, J.J. Zou, X.W. Zhang, L. Wang, Indust.Eng. Chem. Res. **49**, 8526 (2010).
[28] A. Zielinska, E. Kowalska, J.W. Sobczak, I. Lacka, M. Gazda, B. Ohtani, J. Hupka, A.Zaleska, Sep. Purif. Technol. **72**, 309 (2010).
[29] M. Zou, L. Feng, A. S. Ganeshraja, F. Xiong, M. Yang, Solid State Sci. **60**, 1 (2016).
[30] M. Yanga, L. Huoa, L. Peia, K. Panb, Y. Gan, Electrochim. Acta. **125**, 288 (2014).
[31] S. Hu, F. Li, Z. Fan, Bull. Korean Chem. Soc. **33**, 4052 (2012).
[32] J. Yang, H. Bai, X. Tan, J. Lian, Appl. Surf. Sci. **253**, 1988 (2006)
[33] F. Chenga, S.M. Sajedina, S.M. Kellya, A.F. Lee, A. Kornherr, Carbohydr. Polym.**114**, 246 (2014).
[34] J. Zhu, Z. Deng, F. Chen, J. Zhang, H. Chen, M. Anpo, J. Huang, L. Zhang, Appl. Catal. B: Environ. **62**, 329 (2006).
[35] Q. Xiao, Z.C. Si, J. Zhang, C. Xiao, X.K. Tan, J. Hazard. Mater. **150**, 62 (2008).
[36] N. Sobana, M. Muruganadham, M. Swaminathan, J. Mol. Catal. A: Chem. **258,** 124 (2006).
[37] S. Paul, A. Choudhury, S. Bojja, Micro. Nano. Lett. **8(4)**, 184 (2013).
[38] L.G. Devi, N. Kottam, S.G. Kumar, K.E. Rajashekhar, Cent. Eur. J. Chem. **8**(1), 142 (2010).
[39] L.G. Devi, N. Kottam, B.N. Murthy, S.G. Kumar, J. Molecular Catal. A: Chem. **328,** 44 (2010).